

A Stabilization of a Continuous Limit of the Ensemble Kalman Inversion

Dieter Armbruster

*School of Mathematical and Statistical Sciences
Arizona State University
Tempe, AZ 85287-1804, USA*

Michael Herty

*Institut für Geometrie und Praktische Mathematik (IGPM)
RWTH Aachen University
Templergraben 55, 52062 Aachen, Germany*

Giuseppe Visconti

*Dipartimento di Matematica “G. Castelnuovo”
La Sapienza, Università di Roma
P.le Aldo Moro 5, 00185 Roma, Italy*

June 21, 2022

Abstract

The Ensemble Kalman Filter (EnKF) belongs to the class of iterative particle filtering methods and can be used for solving control-to-observable inverse problems. In this context, the EnKF is known as Ensemble Kalman Inversion (EKI). In recent years several continuous limits in the number of iteration and particles have been performed in order to study properties of the method. In particular, a one-dimensional linear stability analysis reveals possible drawbacks in the phase space of moments provided by the continuous limits of the EKI, but observed also in the multi-dimensional setting. In this work we address this issue by introducing a *stabilization* of the dynamics which leads to a method with globally asymptotically stable solutions. We illustrate the performance of the stabilized version by using test inverse problems from the literature and comparing it with the classical continuous limit formulation of the method.

Mathematics Subject Classification (2010) Dynamical systems, inverse problems, regularization, stabilization, nonlinear filtering methods, moment equations

Keywords 37N35 (Dynamical systems in control), 65N21 (Inverse problems), 93E11 (Filtering)

1 Introduction

In this paper we investigate a particular numerical method for solving inverse problems, namely, the Ensemble Kalman Inversion (EKI), originally introduced in [23]. This method can be derived in the framework of the Ensemble Kalman Filter (EnKF) as briefly explained later in this introduction and in Section 2. While the EnKF has already been introduced more than ten years ago [4, 11, 14, 15] as a discrete time method to estimate state variables and parameters of stochastic dynamical systems, the EKI has been recently and successfully applied to solve inverse problems in many research fields due to its derivative-free structure, in particular in oceanography [16], reservoir modeling [1], weather forecasting [24], milling process [29], process control [31], and also machine learning [20, 25].

In order to set up the mathematical formulation, we let $\mathcal{G} : X \rightarrow Y$ be the given (possible nonlinear) forward operator between the Euclidean spaces $X = \mathbb{R}^d$, $d \in \mathbb{N}$, and $Y = \mathbb{R}^K$, $K \in \mathbb{N}$. We are concerned with the following abstract inverse problem or parameter identification problem

$$(1) \quad \mathbf{y} = \mathcal{G}(\mathbf{u}) + \boldsymbol{\eta}$$

aiming to recover unknown control $\mathbf{u} \in X$ from given observations $\mathbf{y} \in Y$, where $\boldsymbol{\eta}$ is observational noise. Typically, $d \gg K$ and $\boldsymbol{\eta}$ is not explicitly known but only information on its distribution is available. We assume that $\boldsymbol{\eta} \sim \mathcal{N}(\mathbf{0}, \Gamma^{-1})$, i.e. the observational noise is normally distributed with zero mean and given covariance matrix $\Gamma^{-1} \in \mathbb{R}^{K \times K}$.

Relying on the same machinery leading to the EnKF formulation, the EKI can be derived within the inverse problem framework by rewriting (1) as a partially observed and artificial dynamical system based on state augmentation, e.g. cf. [3, 23]. The update formula for each ensemble member is computed by imposing first order necessary optimality conditions to solve a regularized minimization problem, which aims for a compromise between the background estimate of the dynamics model and additional information provided by data model. A similar technique is used to derive the update formula for constrained inverse problems [2, 22].

In order to understand how and why the EKI works, a continuous-time limit [5, 6, 10, 27, 28] and a mean-field limit on the number of the ensemble members [8, 12, 17, 21] have been developed. Continuous-limits have been performed also for variants of the EKI, e.g. we refer to [9] for the hierarchical EKI. Recent theoretical progress [21, 27] using these limits in the linear setting is the starting point of the current work. Specifically, it has been shown that, within these limits and assuming a linear forward model, the EKI provides a solution to the inverse problem (1) by minimizing the least-squares functional

$$(2) \quad \Phi(\mathbf{u}, \mathbf{y}) := \frac{1}{2} \left\| \Gamma^{\frac{1}{2}}(\mathbf{y} - \mathcal{G}(\mathbf{u})) \right\|_Y^2$$

via a preconditioned gradient flow equation, where the preconditioner is given by the empirical covariance of the ensemble, in the continuous-time limit, and via a Vlasov-type equation in the mean-field limit. Note that, contrary to the fully discrete and classical formulation of the EKI, there is no regularization of the control \mathbf{u} in the minimization of (2). However, when the inverse problem is ill-posed, infimization of Φ is not a well-posed problem and some form of regularization may be required. This has been recognized in [10, 34] where

modifications of the EKI are proposed, leading to Tikhonov–Phillips–like regularizations of (2).

Another source of problems is given by the preconditioned gradient flow structure and can be analyzed with the system of the first and second central moment, i.e. the expected value and the variance of the distribution of the ensemble, respectively. In [21] a one–dimensional linear stability analysis of the moment equations resulting from the mean–field limit revealed that the method has infinitely many non–hyperbolic Bogdanov–Takens equilibria [18]. In this work, we provide also the evidence that this structure of the phase space is kept in the multi–dimensional setting. Although it is possible to show that the equilibrium providing the minimization of (2) is still a global attractor, having infinitely many non–hyperbolic equilibria leads to several undesirable consequences. In fact, not only are Bogdanov–Takens equilibria not asymptotically stable they are structurally unstable and thus non robust and extremely sensitive to model perturbations. These equilibria lie on the set where the preconditioner collapse to zero. Thus, convergence to the solution of the minimization of (2) may be affected by numerical instability which may occur, e.g., due to an overly confident prior, i.e. when the initial ensemble is characterized by a small variance. Numerical and practical instability may either push the trajectory in the unfeasible region of the phase space, i.e. where the variance of the ensemble is negative, or get the method stuck in the wrong equilibrium. These observations would therefore lead to the necessity of employing a proper and robust numerical discretization of the method. Furthermore, the presence of non–hyperbolic equilibria leads to a slow convergence of the method to the equilibrium solution, which happens at the rate $\mathcal{O}(t^{-1})$ where t represents the time.

In this work we address these issues by introducing a modification of the continuous dynamics for the ensemble, in such a way that the corresponding phase plane of the moment equations is characterized by a globally asymptotically stable equilibrium, the one minimizing the least–squares functional (2). The stabilization effect is obtained by artificially inflating the preconditioner of the gradient flow equation with an additive term which acts as a regularization. The advantage is twofold. First, the new phase space of moments is robust. Instead, in the limits of the classical EKI, a small perturbation into the unfeasible region explodes, bringing the trajectory far from the desired one. Second, as consequence of the stabilization, the rate of convergence to the solution of the minimization of (2) is improved, resulting now exponentially fast. In addition, we consider a suitable acceleration/relaxation term aiming to control the distance of each ensemble member to their mean. This term further speeds up the convergence rate. The usual properties of the classical ensemble Kalman inversion, such as decay of the ensemble spread, are still satisfied by this stabilized version of the method. Its performance is investigated for a two–dimensional inverse problem. We show that the new method is able to converge to the solution faster and, more importantly, converges independently of the properties of the initial ensemble. Although the analysis focuses on linear forward models, numerical examples seem to suggest that the stabilization we propose provides advantages also when applied to nonlinear inverse problems. For further evidences on why EKI formulations perform well in nonlinear settings we refer to [13].

We point out that, although the instability discussed above is not observed in the discrete version of the EKI, for practical purposes it is still crucial to introduce a stabilization of the continuous limits. In fact, the mean–field limit can be particularly useful in applications because it allows to describe the case of infinitely many ensemble members and to guarantee a computational gain in the numerical simulations using fast techniques, e.g. see [17, 21, 29].

The rest of the paper is organized as follows. In Section 2 we review the ensemble Kalman filter formulation for inverse problems and the continuous formulations. In particular, the linear stability analysis of the moment equations performed in [21] is recalled. In Section 3 we discuss the stabilization of the dynamics and analyze the properties of the regularized method. In Section 4 we investigate the ability of the method to provide solution to an inverse problem based on a two-dimensional elliptic PDE. Finally, we summarize the results in Section 5.

2 Preliminaries on the Ensemble Kalman Inversion

We briefly recall the original formulation of the Ensemble Kalman Inversion (EKI), cf. [23], which is based on a sequential update of an ensemble to estimate the solution of control-to-observable inverse problems. The derivation of the method is presented within optimization theory considering only the deterministic version of EKI, i.e. without artificial random perturbation of the measurement during the iteration in time. Focusing on recent continuous limit formulations which have allowed theoretical analysis of the nature of the method, we review the one-dimensional linear stability analysis of the moment equations performed in [21].

2.1 Formulation of the Ensemble Kalman Inversion

We consider a number J of ensemble members (realizations of the control $\mathbf{u} \in \mathbb{R}^d$) combined in $\mathbf{U} = \{\mathbf{u}^j\}_{j=1}^J$ with $\mathbf{u}^j \in \mathbb{R}^d$. The EKI is originally posed as a discrete iteration on \mathbf{U} , derived by solving a minimization problem that compromises between the background estimate of the given model and additional information provided by data or measurements. For more details, we refer e.g. to [23]. The iteration index is denoted by n and the collection of the ensemble members by $\mathbf{U}^n = \{\mathbf{u}^{j,n}\}_{j=1}^J$, $\forall n \geq 0$. The EKI iterates each component of \mathbf{U}^n at iteration $n+1$ as

$$(3) \quad \mathbf{u}^{j,n+1} = \mathbf{u}^{j,n} + \mathbf{C}_{\mathcal{G}}(\mathbf{U}^n) \left(\mathbf{D}_{\mathcal{G}}(\mathbf{U}^n) + \frac{1}{\Delta t} \Gamma^{-1} \right)^{-1} (\mathbf{y} - \mathcal{G}(\mathbf{u}^{j,n}))$$

for each $j = 1, \dots, J$, where $\Delta t \in \mathbb{R}^+$ is a parameter. In general, each observation or measurement can be perturbed by additive noise [23]. We focus on the case where the measurement data $\mathbf{y} \in \mathbb{R}^K$ is unperturbed.

The update of the ensemble (3) requires the knowledge of the operators $\mathbf{C}_{\mathcal{G}}(\mathbf{U}^n)$ and $\mathbf{D}_{\mathcal{G}}(\mathbf{U}^n)$ which are, in the present finite dimensional setting, the covariance matrices depending on the ensemble set \mathbf{U}^n at iteration n and on $\mathcal{G}(\mathbf{U}^n)$, i.e. the image of \mathbf{U}^n at iteration n . More precisely, we have

$$(4) \quad \begin{aligned} \mathbf{C}_{\mathcal{G}}(\mathbf{U}^n) &= \frac{1}{J} \sum_{k=1}^J (\mathbf{u}^{k,n} - \bar{\mathbf{u}}^n) (\mathcal{G}(\mathbf{u}^{k,n}) - \bar{\mathcal{G}}^n)^\top \in \mathbb{R}^{d \times K} \\ \mathbf{D}_{\mathcal{G}}(\mathbf{U}^n) &= \frac{1}{J} \sum_{k=1}^J (\mathcal{G}(\mathbf{u}^{k,n}) - \bar{\mathcal{G}}^n) (\mathcal{G}(\mathbf{u}^{k,n}) - \bar{\mathcal{G}}^n)^\top \in \mathbb{R}^{K \times K} \end{aligned}$$

where we define $\bar{\mathbf{u}}^n$ and $\bar{\mathcal{G}}^n$ as the mean of \mathbf{U}^n and $\mathcal{G}(\mathbf{U}^n)$, respectively:

$$\bar{\mathbf{u}}^n = \frac{1}{J} \sum_{j=1}^J \mathbf{u}^{j,n}, \quad \bar{\mathcal{G}}^n = \frac{1}{J} \sum_{j=1}^J \mathcal{G}(\mathbf{u}^{j,n}).$$

The EKI satisfies the subspace property [23], i.e. the ensemble iterates stay in the subspace spanned by the initial ensemble. As consequence, the natural estimator for the solution of the inverse problem is provided by the mean of the ensemble.

2.2 Derivation of the Ensemble Kalman Inversion from an Optimization Point-of-View

The EKI method (3) for the solution of the inverse problem (1) can be derived by using an optimization point-of-view. Below, we briefly review the machinery leading to the EKI formulation. For further details and explicit computations we refer to e.g. [2].

We introduce a new variable $\mathbf{w} = \mathcal{G}(\mathbf{u}) \in \mathbb{R}^K$ and reformulate (1) equivalently as

$$\begin{aligned} \mathbf{w} &= \mathcal{G}(\mathbf{u}) \\ \mathbf{y} &= \mathbf{w} + \boldsymbol{\eta}. \end{aligned}$$

The problem is then reinterpreted as filtering problem by considering a discrete-time dynamical system with state transitions and noisy observations:

$$\begin{aligned} \text{(dynamics model)} \quad & \begin{cases} \mathbf{u}^{n+1} = \mathbf{u}^n \\ \mathbf{w}^{n+1} = \mathcal{G}(\mathbf{u}^n) \end{cases} \\ \text{(data model)} \quad & \mathbf{y} = \mathbf{w}^{n+1} + \boldsymbol{\eta}. \end{aligned}$$

By defining $\mathbf{v} = [\mathbf{u}, \mathbf{w}]^T \in \mathbb{R}^{d+K}$ and $\Xi : \mathbf{v} \mapsto \Xi(\mathbf{v}) = [\mathbf{u}, \mathcal{G}(\mathbf{u})]^T \in \mathbb{R}^{d+K}$, the dynamical model can be written as

$$\mathbf{v}^{n+1} = \Xi(\mathbf{v}^n),$$

whereas the data model becomes

$$\mathbf{y} = \mathbf{H}\mathbf{v}^{n+1} + \boldsymbol{\eta},$$

where $\mathbf{H} = [\mathbf{0}_{K \times d}, \mathbf{I}_{K \times K}] \in \mathbb{R}^{K \times (d+K)}$ is an observation matrix. Let us denote by $\{\mathbf{v}^{j,n}\}_{j=1}^J$ a collection of J ensemble members, also called particles, at time n . The method proceeds as follows.

First, the state of all particles at time $n+1$ is predicted using the dynamical model to give $\{\hat{\mathbf{v}}^{j,n+1}\}_{j=1}^J$, i.e. $\hat{\mathbf{v}}^{j,n+1} = \Xi(\mathbf{v}^{j,n})$. The resulting empirical covariance $\mathbf{Cov} \in \mathbb{R}^{(d+K) \times (d+K)}$ of the uncertainties in the predictions is computed. Exploiting the definition of Ξ it is easy to check that

$$\mathbf{Cov} = \frac{1}{J} \sum_{k=1}^J (\hat{\mathbf{v}}^{k,n+1} - \bar{\hat{\mathbf{v}}}^{n+1})(\hat{\mathbf{v}}^{k,n+1} - \bar{\hat{\mathbf{v}}}^{n+1})^\top = \begin{bmatrix} \mathbf{C} & \mathbf{C}_{\mathcal{G}} \\ \mathbf{C}_{\mathcal{G}}^\top & \mathbf{D}_{\mathcal{G}} \end{bmatrix},$$

where $\mathbf{C}_{\mathcal{G}}$ and $\mathbf{D}_{\mathcal{G}}$ are as in (4), whereas

$$\mathbf{C} = \frac{1}{J} \sum_{k=1}^J (\mathbf{u}^{k,n} - \bar{\mathbf{u}}^n)(\mathbf{u}^{k,n} - \bar{\mathbf{u}}^n)^\top \in \mathbb{R}^{d \times d}.$$

Then, the update $\mathbf{v}^{j,n+1}$ of each particle is determined by imposing first order necessary optimality condition of the following minimization problem

$$\mathbf{v}^{j,n+1} = \arg \min_{\mathbf{v}} \mathcal{J}^{j,n}(\mathbf{v}),$$

which is solved sequentially, and where $\mathcal{J}^{j,n}(\mathbf{v})$ is the objective function which encapsulates the model–data compromise:

$$(5) \quad \mathcal{J}^{j,n}(\mathbf{v}) = \frac{1}{2} \|\mathbf{y}^{n+1} - \mathbf{H}\mathbf{v}\|_{\Gamma^{-1}}^2 + \frac{1}{2} \|\mathbf{v} - \hat{\mathbf{v}}^{j,n+1}\|_{\mathbf{Cov}}^2.$$

Finally, the update (3) of $\mathbf{u}^{j,n+1}$, related to the unknown control state only, is obtained as $\mathbf{H}^\perp \mathbf{v}^{j,n+1}$, with $\mathbf{H}^\perp = [\mathbf{I}_{d \times d}, \mathbf{0}_{d \times K}] \in \mathbb{R}^{d \times (d+K)}$.

This derivation of the ensemble Kalman inversion from an optimization point-of-view leads into the introduction and motivation of the stabilized formulation of the continuous limit. In particular, we observe that the first term of the objective (5) corresponds to the least-squares functional Φ given by (2). Therefore, minimization of (5) can be seen as minimization of Φ subject to a regularization term involving the covariance of the ensemble.

Remark 1. *The derivation of the EKI motivated through the optimization approach assumes that the empirical covariance \mathbf{Cov} is positive definite $\forall n \geq 0$. In general, it is not possible to guarantee that. In [2] and in [6, 32], this issue is overcome by a constant or time dependent shifting of \mathbf{Cov} .*

2.3 Continuous Limits of the Ensemble Kalman Inversion

2.3.1 Continuous-time

As in [27], we compute the continuous-time limit equation of the update (3). We consider the parameter Δt as an artificial time step for the discrete iteration, i.e. $\Delta t \sim N_t^{-1}$ with N_t being the maximum number of iterations and define $\mathbf{U}^n \approx \mathbf{U}(n\Delta t) = \{\mathbf{u}^j(n\Delta t)\}_{j=1}^J$ for $n \geq 0$. Computing the limit $\Delta t \rightarrow 0^+$ we obtain

$$(6) \quad \begin{aligned} \frac{d}{dt} \mathbf{u}^j &= \mathbf{C}_G(\mathbf{U}) \Gamma(\mathbf{y} - \mathcal{G}(\mathbf{u}^j)), \quad j = 1, \dots, J \\ \mathbf{C}_G(\mathbf{U}) &= \frac{1}{J} \sum_{k=1}^J (\mathbf{u}^k - \bar{\mathbf{u}})(\mathcal{G}(\mathbf{u}^k) - \bar{\mathcal{G}})^\top \end{aligned}$$

with initial condition $\mathbf{U}(0) = \mathbf{U}^0$.

Linear forward model

Let us consider the case of \mathcal{G} linear, i.e. $\mathcal{G}(\mathbf{u}) = \mathbf{G}\mathbf{u}$, with $\mathbf{G} \in \mathbb{R}^{K \times d}$. Then (6) is a gradient descent equation and we can write $\mathbf{C}_G(\mathbf{U}) = \frac{1}{J} \sum_{k=1}^J (\mathbf{u}^k - \bar{\mathbf{u}})(\mathbf{u}^k - \bar{\mathbf{u}})^\top \mathbf{G}^\top$. Since the least-squares functional (2) yields

$$(7) \quad \nabla_{\mathbf{u}} \Phi(\mathbf{u}, \mathbf{y}) = -\mathbf{G}^\top \Gamma(\mathbf{y} - \mathbf{G}\mathbf{u}),$$

equation (6) can be stated in terms of the gradient of Φ as

$$(8) \quad \begin{aligned} \frac{d}{dt} \mathbf{u}^j &= -\mathbf{C}(\mathbf{U}) \nabla_{\mathbf{u}} \Phi(\mathbf{u}^j, \mathbf{y}), \quad j = 1, \dots, J \\ \mathbf{C}(\mathbf{U}) &= \frac{1}{J} \sum_{k=1}^J (\mathbf{u}^k - \bar{\mathbf{u}})(\mathbf{u}^k - \bar{\mathbf{u}})^\top. \end{aligned}$$

Equation (8) describes a preconditioned gradient descent equation for each ensemble aiming to minimize Φ . $\mathbf{C}(\mathbf{U})$ is positive semi-definite and hence

$$(9) \quad \frac{d}{dt} \Phi(\mathbf{u}(t), \mathbf{y}) = \frac{d}{dt} \frac{1}{2} \left\| \Gamma^{\frac{1}{2}} (\mathbf{y} - \mathbf{G}\mathbf{u}) \right\|^2 \leq 0.$$

Although the forward operator is assumed to be linear, the gradient flow is nonlinear. For further details and properties of the gradient descent equation (8) we refer to [27]. In particular, the subspace property of the EKI also holds for the continuous dynamics.

Note that, in the continuous-time limit a term originally present in the fully-discrete EKI method (3) is lost, cf. (3). This is due to the scaling assumption of the measurement covariance by Δt which makes the term of order Δt^2 vanishing in the limit $\Delta t \rightarrow 0^+$. This term is however not a Tikhonov regularization-type term but may act as regularization term. We will come back to this point in the next sections.

2.3.2 Mean-field

By definition, the EKI method is a computational method and hence is calculated for a finite ensemble size. The behavior of the method in the limit of infinitely many ensembles can be studied via mean-field limit leading to a Vlasov-type kinetic equation for the compactly supported on \mathbb{R}^d probability density of \mathbf{u} at time t , denoted by

$$(10) \quad f = f(t, \mathbf{u}) : \mathbb{R}^+ \times \mathbb{R}^d \rightarrow \mathbb{R}^+.$$

First we show the limit equation for the case of a non-linear model and later specialize it to a linear model \mathbf{G} . We follow the classical formal derivation to formulate a mean-field equation of a particle system, see [7, 19, 26, 33]. We introduce the first moments $\mathbf{m} \in \mathbb{R}^d$, $\mathbf{m}_{\mathcal{G}} \in \mathbb{R}^K$ and the second moments $\mathbf{E} \in \mathbb{R}^{d \times d}$, $\mathbf{E}_{\mathcal{G}} \in \mathbb{R}^{d \times K}$ of f at time t , respectively, as

$$(11) \quad \begin{aligned} \mathbf{m}(t) &= \int_{\mathbb{R}^d} \mathbf{u} f(t, \mathbf{u}) d\mathbf{u}, & \mathbf{E}(t) &= \int_{\mathbb{R}^d} \mathbf{u} \otimes \mathbf{u} f(t, \mathbf{u}) d\mathbf{u}, \\ \mathbf{m}_{\mathcal{G}}(t) &= \int_{\mathbb{R}^d} \mathcal{G}(\mathbf{u}) f(t, \mathbf{u}) d\mathbf{u}, & \mathbf{E}_{\mathcal{G}}(t) &= \int_{\mathbb{R}^d} \mathbf{u} \otimes \mathcal{G}(\mathbf{u}) f(t, \mathbf{u}) d\mathbf{u}. \end{aligned}$$

Since $\mathbf{u} \in \mathbb{R}^d$, the corresponding discrete measure on the ensemble set $\mathbf{U} = \{\mathbf{u}^j\}_{j=1}^J$ is given by the empirical measure

$$(12) \quad f(t, \mathbf{u}) = \frac{1}{J} \sum_{j=1}^J \delta(\mathbf{u}^j - \mathbf{u}).$$

Let us consider the interacting particle system (6). The empirical measure allows for a mean-field limit of $\mathbf{C}_{\mathcal{G}}$ as

$$(\mathbf{C}_{\mathcal{G}})_{\kappa,\ell} = \int_{\mathbb{R}^d} u_{\kappa} \mathcal{G}(u)_{\ell} f(t, \mathbf{u}) d\mathbf{u} - \int_{\mathbb{R}^d} u_{\kappa} f(t, \mathbf{u}) d\mathbf{u} \int_{\mathbb{R}^d} \mathcal{G}(u)_{\ell} f(t, \mathbf{u}) d\mathbf{u}, \quad \kappa, \ell = 1, \dots, d$$

and therefore $\mathbf{C}_{\mathcal{G}}$ can be written in terms of the moments (11) of f only as

$$(13) \quad \mathbf{C}_{\mathcal{G}}(f) = \mathbf{E}_{\mathcal{G}}(t) - \mathbf{m}(t) \mathbf{m}_{\mathcal{G}}^T(t) \geq 0.$$

We denote a sufficiently smooth test function by $\varphi(\mathbf{u}) \in C_0^1(\mathbb{R}^d)$ and compute

$$\begin{aligned} \frac{d}{dt} \langle f, \varphi \rangle &= \frac{d}{dt} \int_{\mathbb{R}^d} \frac{1}{J} \sum_{j=1}^J \delta(\mathbf{u} - \mathbf{u}^j) \varphi(\mathbf{u}) d\mathbf{u} = -\frac{1}{J} \sum_{j=1}^J \nabla_{\mathbf{u}} \varphi(\mathbf{u}^j) \cdot \mathbf{C}_{\mathcal{G}}(f) \Gamma(\mathbf{y} - \mathcal{G}(\mathbf{u}^j)) \\ &= - \int_{\mathbb{R}^d} \nabla_{\mathbf{u}} \varphi(\mathbf{u}) \cdot \mathbf{C}_{\mathcal{G}}(f) \Gamma(\mathbf{y} - \mathcal{G}(\mathbf{u})) f(t, \mathbf{u}) d\mathbf{u} \end{aligned}$$

which finally leads to the strong form of the mean-field kinetic equation corresponding to the continuous-time limit (6):

$$(14) \quad \partial_t f(t, \mathbf{u}) - \nabla_{\mathbf{u}} \cdot (\mathbf{C}_{\mathcal{G}}(f) \Gamma(\mathbf{y} - \mathcal{G}(\mathbf{u})) f(t, \mathbf{u})) = 0.$$

Linear forward model

In case of a linear model $\mathcal{G}(\cdot) = \mathbf{G} \cdot$, which is the assumption we use for the subsequent analysis, the mean-field kinetic equation corresponding to the gradient descent equation (8) becomes

$$(15) \quad \partial_t f(t, \mathbf{u}) - \nabla_{\mathbf{u}} \cdot (\mathbf{C}(f) \nabla_{\mathbf{u}} \Phi(\mathbf{u}, \mathbf{y}) f(t, \mathbf{u})) = 0.$$

where, similarly to $\mathbf{C}_{\mathcal{G}}(f)$, the operator $\mathbf{C}(f)$ can be also defined in terms of moments of the empirical measure (12) as

$$(16) \quad \mathbf{C}(f) = \mathbf{E}(t) - \mathbf{m}(t) \mathbf{m}^T(t) \geq 0.$$

For the rigorous mean-field derivation and analysis of the EKI we refer to [8, 12].

We observe that (15) is a nonlinear transport equation arising from non-linear gradient flow interactions and the counterpart of (9) holds at the kinetic level. Defining

$$\mathcal{L}(f, \mathbf{y}) = \int_{\mathbb{R}^d} \Phi(\mathbf{u}, \mathbf{y}) f(t, \mathbf{u}) d\mathbf{u}$$

we compute

$$\frac{d}{dt} \mathcal{L}(f, \mathbf{y}) = \int_{\mathbb{R}^d} \Phi(\mathbf{u}, \mathbf{y}) \partial_t f(t, \mathbf{u}) d\mathbf{u} = - \int_{\mathbb{R}^d} (\nabla_{\mathbf{u}} \Phi(\mathbf{u}, \mathbf{y}))^T \mathbf{C}(f) \nabla_{\mathbf{u}} \Phi(\mathbf{u}, \mathbf{y}) d\mathbf{u} \leq 0$$

since $\mathbf{C}(f)$ is positive semi-definite. In particular, $\mathcal{L}(f, \mathbf{y})$ is decreasing unless f is a Dirac distribution. This reveals that a solution of $\min_{\mathbf{u} \in \mathbb{R}^d} \Phi(\mathbf{u}, \mathbf{y})$ provides a steady solution of the continuous-limit formulation, but the converse is not necessarily true. In fact, all Dirac distributions, i.e. all f satisfying $\mathbf{C}(f) = 0$, provide steady solutions of (15). In particular, the velocity of convergence to the *correct* Dirac distribution may be highly influenced by the initial properties of the initial condition, i.e. by the distribution of the initial ensemble.

2.4 Stability of the Moment Equations

The previous observations are in-depth investigated at the level of moments of the mean-field equation, in order to gain insights on the nature of the steady states. We recall that the expected value of the ensemble is selected as estimator for the solution, due to the subspace property satisfied by the EKI. For this reason the analysis of moments is of crucial importance in order to understand the properties of the method.

In [21], the linear stability analysis of the moment equations resulting from (15) has been investigated for one-dimensional controls. Here, we briefly review, but also extend, that analysis. First, we restrict the attention to the case $d = K = 1$. From now on, we avoid using bold font to emphasize that the involved quantities are one-dimensional.

The dynamical system for the first and second moment is computed from (15). Using the linearity of the model we obtain

$$(17) \quad \begin{aligned} \frac{d}{dt}m(t) &= C(m, E)G^T\Gamma(y - Gm) \\ \frac{d}{dt}E(t) &= 2C(m, E)G^T\Gamma(y m - GE), \end{aligned}$$

where we observe that $C(m, E)$ corresponds to the variance, in fact

$$\int_{\mathbb{R}} (u - m(t))^2 f(t, u) du = E(t) - m(t)^2.$$

System (17) is closed by the second moment equation due to the assumption of a linear model. If the forward model were nonlinear, then the knowledge of the dynamics of the mixed moments in (11) would be required to have a closed hierarchy.

We analyze steady-states and their stability with $G = \Gamma = 1$. Nullclines of (17) are given by

$$\begin{aligned} \frac{d}{dt}m(t) = 0 &\Leftrightarrow m = y \vee E = m^2 \\ \frac{d}{dt}E(t) = 0 &\Leftrightarrow E = ym \vee E = m^2. \end{aligned}$$

Equilibrium points arise by intersection of the nullclines and are thus

$$(18) \quad F_k = (k, k^2), \quad k \in \mathbb{R},$$

i.e. all equilibria are points on the set $E = m^2$ for which $C = 0$. We note that they lie on the boundary of the admissible region $C \geq 0$. This means that all Dirac delta distributions are steady-states of the mean-field equation, as shown for cases of arbitrary dimension at the end of Section 2.3. As consequence we have a set of infinitely many steady-states. The one minimizing the least square functional Φ is $\delta(u - y)$, corresponding to $F_y = (y, y^2)$. Studying the linear (in)stability of the equilibrium points, it is simple to show that all the F_k 's have double-zero eigenvalues and, thus are non-hyperbolic Bogdanov-Takens-type equilibria.

Nevertheless, we point out that the desired steady state F_y , although being a Bogdanov-Takens equilibrium, is still a global attractor of the dynamics when the initial condition belongs to the region $C > 0$. In order to show this, consider the coupled system of ODEs for m

and $C = E - m^2$, with $G = \Gamma = 1$:

$$\begin{aligned}\frac{d}{dt}m(t) &= C(y - m) \\ \frac{d}{dt}C(t) &= -2C^2.\end{aligned}$$

Then, we observe that, on the region $C > 0$, $\dot{m} > 0$ for $m < y$ and $\dot{m} < 0$ for $m > y$. Instead, $\dot{C} < 0$ for all C . The trajectories in the phase space (m, C) can be computed by solving

$$\frac{d}{dm}C(m) = -2\frac{C}{(y - m)}$$

which gives $C(m) = c(m - y)^2$, with c an integration constant. This proves that the equilibrium $(m, C) = (y, 0)$, which corresponds to F_y in the phase space (m, E) , is the global attractor for all initial conditions $C > 0$.

However, having non-hyperbolic equilibria has several undesirable consequences: Bogdanov–Takens equilibria are not asymptotically stable, in fact their linearization is unstable. More importantly, they are non-hyperbolic and thus structurally unstable, i.e. susceptible to qualitative changes under arbitrary small perturbations of the underlying model. In addition, the instability of the phase space may result also in numerical instabilities leading trajectories to the unfeasible region, i.e. where $C(m, E) < 0$, or to get stuck in an equilibrium point which is not F_y . Finally, we may face a slow convergence to the global attractor equilibrium. In fact, we notice that the differential equation for C can also be solved explicitly, giving us

$$C(t) = \frac{C(0)}{1 + 2C(0)t},$$

with $C(0)$ being the initial condition. Thus, $C(t) \rightarrow 0^+$, as $t \rightarrow +\infty$, very slowly, precisely with rate $\mathcal{O}(t^{-1})$.

2.4.1 Stability for Multi-Dimensional Controls

We recall that the existence of infinitely many steady-states satisfying $\mathbf{C} = 0$ holds in general dimension, as observed in Section 2.3.2. Instead, the above stability analysis is performed in the simplest setting $d = 1$. However, here we provide a numerical evidence that the nature of the equilibria lying in the kernel of \mathbf{C} is maintained also in general dimension, i.e. when $d > 1$.

Let $\mathbf{y} \in \mathbb{R}^d$ and consider the $d + d^2$ dynamical system

$$(19) \quad \begin{aligned}\frac{d}{dt}\mathbf{m}(t) &= (\mathbf{E} - \mathbf{m}\mathbf{m}^T)(\mathbf{y} - \mathbf{m}) \\ \frac{d}{dt}\mathbf{E}(t) &= 2(\mathbf{E} - \mathbf{m}\mathbf{m}^T)(\mathbf{y}\mathbf{m}^T - \mathbf{E}),\end{aligned}$$

where $\mathbf{m} \in \mathbb{R}^d$ and $\mathbf{E} \in \mathbb{R}^{d \times d}$. We are interested in the equilibrium points $(\mathbf{m}^*, \mathbf{E}^*)$ such that $\mathbf{C}^* := \mathbf{E}^* - \mathbf{m}^*(\mathbf{m}^*)^T = \mathbf{0}$. To this end, it is convenient to rewrite, equivalently, the dynamical

system (19) in terms of \mathbf{m} and $\mathbf{C} = \mathbf{E} - \mathbf{m}\mathbf{m}^T \in \mathbb{R}^{d \times d}$ as

$$\begin{aligned}
(20) \quad \frac{d}{dt}\mathbf{m}(t) &= \mathbf{C}(\mathbf{y} - \mathbf{m}) \\
\frac{d}{dt}\mathbf{C}(t) &= \frac{d}{dt}\mathbf{E} - \frac{d}{dt}\mathbf{m}\mathbf{m}^T - \mathbf{m}\frac{d}{dt}\mathbf{m}^T \\
&= \mathbf{C}\mathbf{y}\mathbf{m}^T - \mathbf{m}\mathbf{y}^T\mathbf{C}^T - 2\mathbf{C}\mathbf{C} - \mathbf{C}\mathbf{m}\mathbf{m}^T + \mathbf{m}\mathbf{m}^T\mathbf{C}^T \\
&= -2\mathbf{C}\mathbf{C} + \mathbf{C}\mathbf{A} - \mathbf{A}^T\mathbf{C}^T,
\end{aligned}$$

where $\mathbf{A} := \mathbf{y}\mathbf{m}^T - \mathbf{m}\mathbf{m}^T$.

It is clear that $\mathbf{C} = \mathbf{0}$ defines a set of equilibrium points of (20). By linearization we compute the Jacobian matrix

$$\mathbf{J} = \begin{bmatrix} \mathbf{J}_{11} & \mathbf{J}_{12} \\ \mathbf{J}_{21} & \mathbf{J}_{22} \end{bmatrix} \in \mathbb{R}^{(d+d^2) \times (d+d^2)}$$

where the four blocks are

$$\begin{aligned}
\mathbf{J}_{11} &= \frac{\partial \dot{\mathbf{m}}}{\partial \mathbf{m}} \in \mathbb{R}^{d \times d}, \quad \mathbf{J}_{12} = \frac{\partial \dot{\mathbf{m}}}{\partial \mathbf{C}} \in \mathbb{R}^{d \times d^2}, \\
\mathbf{J}_{21} &= \frac{\partial \dot{\mathbf{C}}}{\partial \mathbf{m}} \in \mathbb{R}^{d^2 \times d}, \quad \mathbf{J}_{22} = \frac{\partial \dot{\mathbf{C}}}{\partial \mathbf{C}} \in \mathbb{R}^{d^2 \times d^2}.
\end{aligned}$$

Then, on $\mathbf{C} = \mathbf{0}$ we have $\mathbf{J}_{11} = -\mathbf{C} = \mathbf{0}$ and, similarly, $\mathbf{J}_{21} = \mathbf{0}$ since it is quadratic with respect to \mathbf{C} . Instead,

$$\mathbf{J}_{12} = [\mathbf{M}_1, \dots, \mathbf{M}_d], \quad \mathbf{M}_i = \mathbf{e}_i(\mathbf{y} - \mathbf{m})^T \in \mathbb{R}^{d \times d}$$

where $\mathbf{e}_i \in \mathbb{R}^d$ is the i -th vector of the standard basis of the Euclidean space \mathbb{R}^d . Then, in general, $\mathbf{J}_{12} \neq \mathbf{0}$ also on $\mathbf{C} = \mathbf{0}$.

The structure of \mathbf{J}_{22} is more involved. However, it is possible to compute the general derivative of $\dot{\mathbf{C}}$ with respect to \mathbf{C} on $\mathbf{C} = \mathbf{0}$ as

$$\frac{\partial \dot{C}_{ij}}{\partial C_{rs}} = \delta_{ir}A_{sj} - \delta_{jr}A_{si}, \quad i, j, r, s = 1, \dots, d,$$

where the δ 's are Kronecker delta functions. In particular, \mathbf{J}_{22} has the following properties

$$\frac{\partial \dot{C}_{ij}}{\partial C_{rs}} = -\frac{\partial \dot{C}_{ji}}{\partial C_{rs}}, \quad \frac{\partial \dot{C}_{ii}}{\partial C_{rr}} = 0.$$

Furthermore, \mathbf{J}_{22} is block structured as

$$\mathbf{J}_{22} = \begin{bmatrix} \mathbf{J}^{11} & \mathbf{J}^{12} & \dots & \mathbf{J}^{1d} \\ \mathbf{J}^{21} & \mathbf{J}^{22} & \dots & \mathbf{J}^{2d} \\ \vdots & \vdots & \ddots & \vdots \\ \mathbf{J}^{d1} & \mathbf{J}^{d2} & \dots & \mathbf{J}^{dd} \end{bmatrix}$$

where $\mathbf{J}^{ir} \in \mathbb{R}^{d \times d}$, $i, r = 1, \dots, d$, with elements $(\mathbf{J}^{ir})_{js} = \frac{d\dot{C}_{ij}}{dC_{rs}}$, $j, s = 1, \dots, d$. Then, the diagonal blocks, i.e. $i = r$, are

$$\mathbf{J}^{ii} = \mathbf{y}\mathbf{m}^T - \mathbf{m}\mathbf{m}^T - \mathbf{D}_i$$

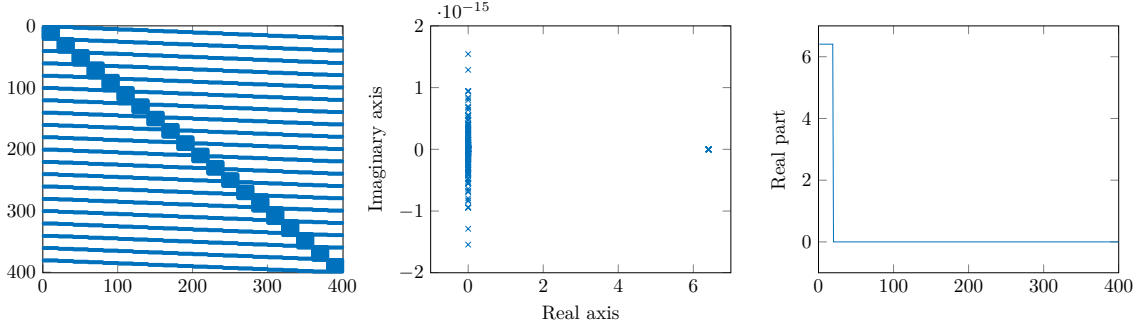


Figure 1: Left: structure of the matrix \mathbf{J}_{22} , where non zero elements are marked by blue dots. Center: eigenvalues of \mathbf{J}_{22} . Right: real part of the eigenvalues of \mathbf{J}_{22} . Here, the dimension is $d = 20$ and the spectral properties are related to $\Phi(\mathbf{u}, \mathbf{y}) = \frac{1}{2} \|\mathbf{y} - \mathbf{u}\|^2$.

where $\mathbf{D}_i \in \mathbb{R}^{d \times d}$ is a null matrix with non-zero elements in row i as $-m_i(\mathbf{y} - \mathbf{m})^T$. Therefore, the blocks \mathbf{J}^{ii} have $d - 1$ linearly dependent rows and rank 2. Whereas, off-diagonal blocks \mathbf{J}^{ir} have all zeros except for the r -th row and thus they are rank 1 blocks. The structure of \mathbf{J}_{22} is shown in the left panel of Figure 1 for the case $d = 20$.

Due to the structure of the Jacobian \mathbf{J} , its eigenvalues are determined by the diagonal blocks \mathbf{J}_{11} and \mathbf{J}_{22} . Numerical evidences suggest that \mathbf{J}_{22} has at least one zero eigenvalue, cf. Figure 1 for the case $d = 20$. Thus, since $\mathbf{J}_{11} = \mathbf{0}$, we conclude that the Jacobian \mathbf{J} has at least $d + 1$ zero eigenvalues on $\mathbf{C} = \mathbf{0}$, corresponding to steady states of Bogdanov–Takens type. This corresponds to the d -dimensional translation symmetry of the data on $\mathbf{C} = \mathbf{0}$ and one additional zero eigenvalue due to a bifurcation. It is the natural extension of the one-dimensional case where we have a double zero eigenvalue due to the same translational symmetry and an additional bifurcation.

3 Stabilization of the Dynamics

Our goal is to introduce a modified formulation of the continuous dynamics in order to make the desired equilibrium $F_y = (y, y^2)$ a globally asymptotically stable equilibrium of the system of moment equations. We are only interested in the equilibrium F_y since the others are irrelevant for the optimization. The modification we propose is inspired by the idea to restore the regularization effect of the discrete EKI which gets lost in the continuous limits.

We propose to consider the following general discrete dynamics for each ensemble member

$j = 1, \dots, J$:

$$\begin{aligned}
\frac{d}{dt} \mathbf{u}^j &= \tilde{\mathbf{C}}_{\mathcal{G}}(\mathbf{U}) \Gamma(\mathbf{y} - \mathcal{G}(\mathbf{u}^j)) + R(\mathbf{U}), \\
R(\mathbf{U}) &= \beta \tilde{\mathbf{C}}(\mathbf{U})(\mathbf{u}^j - \bar{\mathbf{u}}), \\
(21) \quad \tilde{\mathbf{C}}_{\mathcal{G}}(\mathbf{U}) &= \frac{1}{J} \sum_{k=1}^J (\mathbf{u}^k - \kappa \bar{\mathbf{u}}) (\mathcal{G}(\mathbf{u}^k) - \kappa \bar{\mathcal{G}})^\top, \\
\tilde{\mathbf{C}}(\mathbf{U}) &= \frac{1}{J} \sum_{k=1}^J (\mathbf{u}^k - \kappa \bar{\mathbf{u}}) (\mathbf{u}^k - \kappa \bar{\mathbf{u}})^\top,
\end{aligned}$$

with $\kappa, \beta \in \mathbb{R}$. The choices $\kappa = 1$ and $\beta = 0$ yield continuous-time limit (6) for the original ensemble Kalman inversion. Since the analysis of stability of the new dynamics (21) will be performed again in the case of a linear model, now we specialize (21) to this particular setting and then we discuss the role of the modifications we propose.

Linear forward model

The analysis of the proposed stabilization will be also performed in the linear setting $\mathcal{G}(\cdot) = \mathbf{G}\cdot$. Then, (21) becomes

$$\begin{aligned}
\frac{d}{dt} \mathbf{u}^j &= -\tilde{\mathbf{C}}(\mathbf{U}) \nabla_{\mathbf{u}} \Phi(\mathbf{u}^j, \mathbf{y}) + R(\mathbf{U}), \\
R(\mathbf{U}) &= \beta \tilde{\mathbf{C}}(\mathbf{U})(\mathbf{u}^j - \bar{\mathbf{u}}), \\
(22) \quad \tilde{\mathbf{C}}(\mathbf{U}) &= \frac{1}{J} \sum_{k=1}^J (\mathbf{u}^k - \kappa \bar{\mathbf{u}}) (\mathbf{u}^k - \kappa \bar{\mathbf{u}})^\top,
\end{aligned}$$

with Φ being the least-squares functional (2).

The modified dynamics (22) differs from the standard continuous-time limit of the discrete EKI, cf. (8), in the formulation of the preconditioner $\tilde{\mathbf{C}}(\mathbf{U})$ and in the presence of the additive term $R(\mathbf{U})$. The new preconditioner can be thought, for $\kappa > 0$, as inflation of the covariance $\mathbf{C}(\mathbf{U})$ defined in (8). This modification allows us to stabilize the phase space of the moments and κ plays the role of a regularization parameter. The term $R(\mathbf{U})$, instead, can be thought as acceleration/relaxation to equilibrium. This formal presentation of the role of the parameters will be made mathematically rigorous in the following, being the core of the analysis in Section 3.1 and Section 3.2.

We point out that we do not claim uniqueness of the modeling choice of the stabilization term. In fact, we will see that other forms of covariance inflation allow stabilization of the phase space, but they may lead to unbounded choice of the regularization parameter. See Section 3.3.

3.1 Mean-field Limit and Stability Analysis of the Moment Equations

Performing formal computations as in Section 2.3.2, it is possible to show that the solution of the dynamical system (22) satisfies the weak form of the following mean-field equation:

$$(23) \quad \partial_t f(t, \mathbf{u}) - \nabla_{\mathbf{u}} \cdot \left(\tilde{\mathbf{C}}(f) (\nabla_{\mathbf{u}} \Phi(\mathbf{u}, \mathbf{y}) - \beta(\mathbf{u} - \mathbf{m})) f(t, \mathbf{u}) \right) = 0,$$

where $\tilde{\mathbf{C}}(f)$ is the mean-field interpretation of $\tilde{\mathbf{C}}(\mathbf{U})$ in (22). In fact, via the empirical measure (12) we have

$$\begin{aligned} (\tilde{\mathbf{C}}(\mathbf{U}))_{i,\ell} &= \int_{\mathbb{R}^d} u_i u_\ell f(t, \mathbf{u}) d\mathbf{u} \\ &\quad - \kappa(2 - \kappa) \int_{\mathbb{R}^d} u_i f(t, \mathbf{u}) d\mathbf{u} \int_{\mathbb{R}^d} u_\ell f(t, \mathbf{u}) d\mathbf{u}, \quad i, \ell = 1, \dots, d \end{aligned}$$

and therefore it can be written in terms of the moments of f only, leading to

$$\tilde{\mathbf{C}}(f) = \mathbf{E}(t) - \alpha \mathbf{m}(t) \mathbf{m}^\top(t)$$

with $\alpha = \kappa(2 - \kappa)$. Note that, if $\alpha = 1$, $\tilde{\mathbf{C}}(f) \equiv \mathbf{E}(t) - \mathbf{m}(t) \mathbf{m}^\top(t) = \mathbf{C}(f) \geq 0$, see (16), and that $\tilde{\mathbf{C}}$ can be seen as inflation of the covariance \mathbf{C} for $\alpha > 0$, which corresponds to $0 < \kappa < 2$.

The stability of moments is again studied in the simplest setting of a one-dimensional problem, i.e. $d = K = 1$. From (23) we compute

$$\begin{aligned} (24) \quad \frac{d}{dt} m &= \tilde{C}(m, E) G^T \Gamma (y - Gm) \\ \frac{d}{dt} E &= 2\tilde{C}(m, E) (G^T \Gamma (ym - GE) + \beta C(m, E)) \\ \tilde{C}(m, E) &= (E - \alpha m^2) \\ C(m, E) &= (E - m^2), \end{aligned}$$

where we again avoid the use of bold fonts to highlight the one-dimensional quantities.

We introduce the following concepts of admissible initial conditions, solutions and equilibria of (24).

Definition 3.1. *We say that an initial condition of (24) is admissible if $(m(0), E(0)) \in \mathbb{R} \times \mathbb{R}^+$ and $E(0) > m(0)^2$.*

We say that a solution of (24) with admissible initial condition is admissible or belongs to the feasible domain of the phase space (m, E) if $t \in \mathbb{R}^+ \mapsto (m(t), E(t)) \in \mathbb{R} \times \mathbb{R}^+$ satisfies $E(t) \geq m(t)^2$, $\forall t > 0$.

We say that $F = (m_\infty, E_\infty)$ is an admissible or feasible equilibrium point of (24) if $(\dot{m}, \dot{E})|_F \equiv 0$ and $F \in \mathbb{R} \times \mathbb{R}^+$ with $E_\infty \geq m_\infty^2$.

Definition 3.1 can be generalized to the dynamics in general dimension.

Now, we analyze the behavior of the phase portrait of the dynamical system (24).

Proposition 3.2. *Let $(m(0), E(0)) = (m_0, E_0)$ be an admissible initial condition of (24). Assume that $G = \Gamma = 1$. Then, the dynamical system has two feasible equilibrium points, $F_y = (y, y^2)$ and $F_{0,\alpha} = (0, 0)$, $\forall \alpha \in \mathbb{R}$. In particular, $F_{0,\alpha}$ is a non-hyperbolic Bogdanov-Takens equilibrium, and F_y is an asymptotically stable equilibrium, namely $\exists \delta > 0$ such that if $\|(m_0, E_0) - F_y\| < \delta$ then $\lim_{t \rightarrow \infty} (m(t), E(t)) = F_y$, provided $\alpha < 1$ and $\beta < 1$.*

Proof. Steady states are obtained as intersection of the nullclines. For the system (24) with $G = \Gamma = 1$ we get the following equilibrium points (m, E) :

$$(25) \quad F_y = (y, y^2), \quad F_{k,\alpha} = (k, \alpha k^2), \quad k \in \mathbb{R}.$$

By the Hartman–Grobman Theorem, non-linear dynamical systems are locally topologically conjugate to their linearized formulations near hyperbolic fixed point. Thus, if F_y is hyperbolic and asymptotically stable, the local phase portrait of the non-linear system (24) is equivalent to that of its linearization $[\dot{m}, \dot{E}]^T = \mathbf{J}(m, E)[m, E]^T$, where $\mathbf{J}(m, E)$ is the Jacobian. The eigenvalues of the Jacobian evaluated at the equilibrium point F_y are

$$(26) \quad \lambda_1^{F_y} = y^2(\alpha - 1), \quad \lambda_2^{F_y} = -2y^2(\beta - 1)(\alpha - 1),$$

therefore F_y is an asymptotically stable equilibrium if $\alpha < 1$ and $\beta < 1$. We notice that $\alpha < 1$ automatically implies that, except for $k = 0$, all the other equilibria $F_{k,\alpha}$ are not feasible since then $C(m, E) < 0$. In addition, $F_{0,\alpha}$ is still a Bogdanov–Takens–type equilibrium, and thus unstable, since its eigenvalues are $\lambda_{1,2}^{F_{0,\alpha}} = 0$. \square

The previous result shows that α plays the role of a bifurcation parameter. In fact, for $\alpha \rightarrow 1$ we recover the same equilibria and topological behavior in the phase space as in the classical continuous-limits of the ensemble Kalman inversion, cf. (18). In particular, α allows to stabilize the dynamics. The new ensemble update (22) still has infinitely many equilibria but on the set $E = \alpha m^2$, which lies in the unfeasible region of the phase space for $\alpha < 1$. In addition, for this choice of α , (18) has F_y as isolated hyperbolic and asymptotically stable fixed point of the dynamics.

Remark 2 (Lower bound for α). *We observe that we have not discussed the stability of the equilibrium points $F_{k,\alpha}$, since the choice $\alpha < 1$ makes them unfeasible. If we impose that they are unstable, then we need additional constraints on α and β . The eigenvalues of a point $F_{k,\alpha}$, $k \in \mathbb{R} \setminus \{0\}$, are*

$$\lambda_1^{F_{k,\alpha}} = 0, \quad \lambda_2^{F_{k,\alpha}} = 2k(y - k\beta)(1 - \alpha).$$

Thus, these points are still non-hyperbolic, saddle-node-type equilibria and unstable from all approaching trajectories if $\beta < \frac{y}{k}$, when $k > 0$, and if $\beta > \frac{y}{k}$, when $k < 0$. In particular, if $k = \frac{y}{\alpha + \beta - \alpha\beta}$, we require that $\alpha \geq 0$, obtaining a lower bound for the bifurcation parameter α .

Finally, we are ready to prove the global asymptotic stability of F_y , which is guaranteed by the following proposition.

Proposition 3.3. *The point $F_y = (y, y^2)$ is a globally asymptotically stable equilibrium of the dynamical system (24) with $G = \Gamma = 1$, namely $\lim_{t \rightarrow \infty} (m(t), E(t)) = F_y$ for any admissible initial condition $(m(0), E(0))$, provided $\alpha < 1$ and $\beta < 1$.*

Proof. To prove global asymptotic stability for F_y we note that the relevant subset of the phase space in \mathbb{R}^2 is bounded by $E = m^2$. It is easy to see that the vector field generated by (24) for $\alpha < 1$ is always pointing inwards, i.e. using a Lyapunov stability argument, there exists a suitable function V defined on $E > m^2$ such that $\frac{d}{dt} V(m, E) < 0$. For instance, take $V(m, E) = (m - y)^2 + (E - y^2)^2$. In addition, for large enough E and $\beta < 1$ solutions do not escape to infinity. Since the only equilibria in this region are on the boundary and since F_y is the only locally stable equilibrium, hence by the Poincaré–Bendixson Theorem we have the statement. \square

3.1.1 Decay Rate

Proposition 3.2 and Proposition 3.3 require $\beta < 1$. Therefore, $R(\mathbf{U})$, introduced in the discrete dynamics (21), is not needed to stabilize the phase portrait since $\beta = 0$ is admissible. Although an optimal, i.e. exponential, rate of convergence is already guaranteed by the fact that the desired equilibrium F_y is globally asymptotically stable, we show in this section that the term $R(\mathbf{U})$ allows to further speed up the convergence to F_y . In particular, we observe an improvement with respect to the rate of convergence obtained by the classical continuous-limit of the EKI, which is $\mathcal{O}(t^{-1})$ as observed at the end of Section 2.4.

We notice that F_y is also a point of the phase space where $C \equiv 0$, as it happens for the classical EKI formulation. Therefore, in order to study the convergence rate to F_y , we study the decay speed of the variance $C(t) = E - m^2$ at 0^+ . For the stabilized version of the ensemble dynamics, cf. (24), we compute

$$\frac{d}{dt}C = \frac{d}{dt}E - 2m \frac{d}{dt}m = -2(1 - \beta)\tilde{C}C \leq -2(1 - \beta)(1 - \alpha)m^2C$$

provided $\beta < 1$. Applying Gronwall inequality we obtain

$$C(t) \leq C(0) \exp\left(-2(1 - \beta)(1 - \alpha) \int_0^t m^2(s) ds\right)$$

which implies exponential rate of decay to 0^+ for $t \rightarrow \infty$. In particular, we observe that the exponential decay can be obtained without the acceleration term $R(\mathbf{U})$ as well, i.e. taking $\beta = 0$, but the decay is faster for $\beta < 0$.

We conclude that, while α plays the role of a bifurcation and stabilization parameter leading to a change of the equilibria in the phase space, β plays the role of a relaxation or acceleration parameter speeding-up the convergence to the desired equilibrium F_y . Therefore, the stabilized EKI proposed in this work has two advantages: it is robust and the approach to the right equilibrium is exponentially fast.

3.2 Properties of the Ensemble Dynamics

It is possible to provide a gradient flow interpretation also for the stabilized dynamics (22). In fact, we observe that each ensemble is solving a preconditioned gradient descent equation of the type

$$\begin{aligned} \frac{d}{dt}\mathbf{u}^j &= -\tilde{\mathbf{C}}(\mathbf{U})\nabla_{\mathbf{u}}\Psi(\mathbf{u}^j, \mathbf{y}, \mathbf{u}^{-j}) \\ \Psi(\mathbf{u}^j, \mathbf{y}, \mathbf{u}^{-j}) &= \Phi(\mathbf{u}^j, \mathbf{y}) - \frac{J\beta}{2(J-1)}\|\mathbf{u}^j - \bar{\mathbf{u}}\|^2, \end{aligned}$$

where we denote $\mathbf{u}^{-j} = \{\mathbf{u}^k\}_{\substack{k=1 \\ k \neq j}}^J$. Within this formulation we see that our modified dynamics again adds a regularization term. Existence and uniqueness of solutions to (22) is straightforward since the right-hand side is locally Lipschitz in \mathbf{u}^j , thus local existence of a solution in the space $\mathcal{C}([0, T])$ holds for some $T > 0$. We need to prove global existence, namely that the solution does not blow up in finite time, and this is guaranteed by Proposition 3.4 below.

We define for each $j = 1, \dots, J$

$$(27) \quad \mathbf{e}^j(t) = \mathbf{u}^j(t) - \bar{\mathbf{u}}(t),$$

$$(28) \quad \mathbf{r}^j(t) = \mathbf{u}^j(t) - \mathbf{u}^*$$

the ensemble spread and the residual to a value \mathbf{u}^* , respectively. Proposition 3.4 gives sufficient conditions for the existence of a monotonic decay for the ensemble spread.

Proposition 3.4. *Let $\mathbf{u}^j(0) \in \mathbb{R}^d$, $j = 1, \dots, J$, be an admissible initial condition of the dynamical system (22). The quantity $\|\mathbf{e}^j(t)\|^2$ is decreasing in time, i.e. $\|\mathbf{e}^j(t)\|^2 \leq \|\mathbf{e}^j(0)\|^2$, for each $j = 1, \dots, J$ and $t \geq 0$, provided that $\alpha < 1$ and $\beta < \min_k \lambda_{\mathbf{G}^T \mathbf{\Gamma} \mathbf{G}}^k$, where $\lambda_{\mathbf{G}^T \mathbf{\Gamma} \mathbf{G}}^k$ denotes the eigenvalues of $\mathbf{G}^T \mathbf{\Gamma} \mathbf{G}$. In particular, if $\mathbf{G}^T \mathbf{\Gamma} \mathbf{G}$ is positive definite then $\lim_{t \rightarrow \infty} \|\mathbf{e}^j(t)\|^2 = 0$.*

Proof. To prove the statement, we proceed similarly to existing theory. Let us denote $\mathbf{I}_d \in \mathbb{R}^{d \times d}$ the identity matrix. The hypothesis $\alpha < 1$ implies $\tilde{\mathbf{C}}$ positive definite for all $t \geq 0$. We compute

$$\frac{1}{2} \frac{d}{dt} \frac{1}{J} \sum_{j=1}^J \|\mathbf{e}^j(t)\|^2 = -\frac{1}{J} \sum_{j=1}^J \langle \mathbf{e}^j(t), \tilde{\mathbf{C}}(t) \mathbf{P}_\beta(t) \mathbf{e}^j(t) \rangle \leq 0$$

where $\mathbf{P}_\beta = \mathbf{G}^T \mathbf{\Gamma} \mathbf{G} - \beta \mathbf{I}_d$. Sufficient condition for the last inequality being strict is $\mathbf{G}^T \mathbf{\Gamma} \mathbf{G}$ positive definite and $\beta < \min_k \lambda_{\mathbf{G}^T \mathbf{\Gamma} \mathbf{G}}^k$. \square

The previous result establishes sufficient conditions for the ensemble collapse to the mean $\bar{\mathbf{u}}$ in the long time behavior, and consequently each ensemble member solves at equilibrium the same minimization problem that $\bar{\mathbf{u}}$ is solving. With this consideration we state and prove the following result on the convergence of the residual in the control space.

Proposition 3.5. *Let $\mathbf{u}^j(0) \in \mathbb{R}^d$, $j = 1, \dots, J$, be an admissible initial condition of the dynamical system (22). Assume that $\mathbf{G}^T \mathbf{\Gamma} \mathbf{G}$ is positive definite and let \mathbf{u}^* be a KKT point of the minimization problem $\min_{\mathbf{u} \in \mathbb{R}^d} \Phi(\mathbf{u}, \mathbf{y})$. Then $\lim_{t \rightarrow \infty} \|\mathbf{r}^j(t)\|^2 = 0$, for each $j = 1, \dots, J$, provided that $\alpha < 1$ and $\beta < \min_k \lambda_{\mathbf{G}^T \mathbf{\Gamma} \mathbf{G}}^k$, where $\lambda_{\mathbf{G}^T \mathbf{\Gamma} \mathbf{G}}^k$ denotes the eigenvalues of $\mathbf{G}^T \mathbf{\Gamma} \mathbf{G}$.*

Proof. By assumption $\mathbf{G}^T \mathbf{\Gamma} \mathbf{G}$ is positive definite and thus we have a unique global minimizer \mathbf{u}^* of the minimization problem $\min_{\mathbf{u} \in \mathbb{R}^d} \Phi(\mathbf{u}, \mathbf{y})$, for a given $\mathbf{y} \in \mathbb{R}^K$. Moreover, for Proposition (3.4) it is sufficient to show that $\|\bar{\mathbf{u}} - \mathbf{u}^*\| \rightarrow 0$ as $t \rightarrow \infty$. The evolution equation of the ensemble mean is given by

$$\frac{d}{dt} \bar{\mathbf{u}} = -\tilde{\mathbf{C}} \nabla_{\mathbf{u}} \Phi(\bar{\mathbf{u}}, \mathbf{y}).$$

Then, since $\tilde{\mathbf{C}}$ is positive definite, at equilibrium the ensemble mean solves the equation $\nabla_{\mathbf{u}} \Phi(\bar{\mathbf{u}}, \mathbf{y}) = 0$. \square

3.3 Other Forms of Stabilization

As already observed, we do not claim uniqueness of the choice of the covariance inflation that is responsible for the stabilization of the dynamics. For the dynamics proposed in this work, the inflation is written as $\tilde{\mathbf{C}} = \mathbf{C} + (1 - \alpha) \mathbf{m}(t) \mathbf{m}^\top(t)$.

Simpler choices may be also considered and may lead to the same stabilization effects. For instance, similarly to [10] in the following we will consider the inflation

$$(29) \quad \tilde{\mathbf{C}} = \mathbf{C} + \varepsilon \mathbf{I},$$

where $\mathbf{I}_d \in \mathbb{R}^{d \times d}$ represents again the identity matrix. Consequently, the one-dimensional system of moments arising from the mean-field equation (23) is

$$\begin{aligned} \frac{d}{dt}m &= \tilde{C}(m, E) G^T \Gamma (y - Gm) \\ \frac{d}{dt}E &= 2\tilde{C}(m, E) \left(G^T \Gamma (ym - GE) + \beta C(m, E) \right) \\ \tilde{C}(m, E) &= (E - m^2 + \varepsilon) \\ C(m, E) &= (E - m^2). \end{aligned}$$

Equilibria are again computed and analyzed by taking $G = \Gamma = 1$. We get

$$\begin{aligned} F_{k, \varepsilon} &= (k, k^2 - \varepsilon), \quad k \in \mathbb{R} \\ F_y &= (y, y^2) \\ F_{\varepsilon, \beta} &= \left(\frac{y \pm \sqrt{y^2 + 4\varepsilon - 4\varepsilon\beta}}{2}, \frac{y \pm y\sqrt{y^2 + 4\varepsilon - 4\varepsilon\beta}}{2} - \varepsilon\beta \right). \end{aligned}$$

The stability of the equilibria is investigated by linearization of the dynamical system around these points. Therefore, the eigenvalues of the corresponding Jacobian matrix are

$$\begin{aligned} \lambda_1^{F_{k, \varepsilon}} &= \lambda_1^{F_{\varepsilon, \beta}} = 0, \quad \lambda_2^{F_{k, \varepsilon}} = \lambda_2^{F_{\varepsilon, \beta}} = 2\varepsilon(1 - \beta) \\ \lambda_1^{F_y} &= -\varepsilon, \quad \lambda_2^{F_y} = -2\varepsilon(1 - \beta). \end{aligned}$$

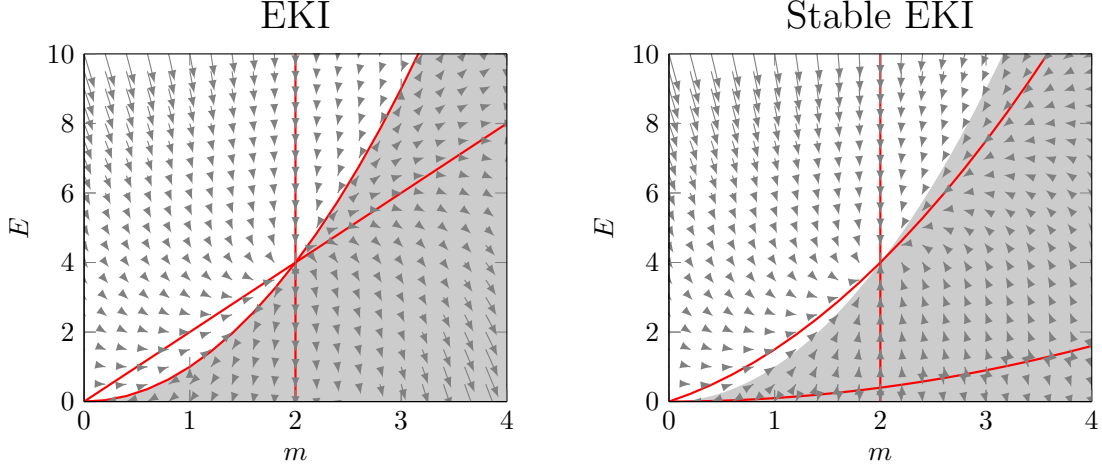
We recall that our goal is to make F_y a globally asymptotically stable equilibrium. This is possible provided $\varepsilon > 0$ and $\beta < 1$. In fact, the requirement $\varepsilon > 0$ makes all the other equilibrium points unfeasible. Also in this case, the term involving the parameter β is not responsible for the stabilization effect since $\beta = 0$ is allowed. Furthermore, exponential decay holds true since

$$C(t) = -\frac{\varepsilon}{1 - \exp(2\varepsilon(1 - \beta)t - \varepsilon c)}$$

with c being integration constant.

However, compared to the dynamics proposed in this work, a simple covariance inflation of the type (29) does not allow for an upper bound of the bifurcation/stabilization parameter ε and this may lead to a large gradient step.

Remark 3. *Alternatively, [21] modified the discrete dynamics with additive white Gaussian noise. This approach leads to a Fokker–Planck–type equation, where Dirac delta distributions are no longer steady states and the desired equilibrium, F_y , depends on the nonzero variance σ of the noise and becomes $(y, y^2 \pm \sqrt{2\sigma^2})$. Therefore, this form of stabilization does not preserve the desired equilibrium.*



(a) The classical ensemble Kalman inversion (17). (b) The stabilized ensemble Kalman inversion (24).

Figure 2: Phase planes of the moment systems. Red lines are nullclines, the gray-shaded area represents the unfeasible region.

4 Numerical Simulations

The simulations performed in this section are all obtained by the numerical solution of the ODE systems for the moments and for the ensemble dynamics. For the sake of simplicity, and also to show that no suitable robust discretization is needed, we straightforwardly employ a first order explicit time integration with a fixed and small time step. We observe that the mean-field limit would also allow to use a fast stochastic particle scheme, e.g. the mean-field interaction algorithm, see [21] for application to the EKI, inspired on Direct Simulation Monte Carlo (DSMC) methods for kinetic equations.

4.1 Simulation of the Moment Dynamics

We recall that the stabilization of the continuous-time limit of the ensemble Kalman inversion is motivated by a linear stability analysis of the moment equations, in the simplest case of a one-dimensional control. For this reason, we aim to compare the moment dynamics provided by the ensemble Kalman inversion (6) and by the present stabilization of the method (21).

All simulations run with the same parameters used for the stability analysis in Section 3.1, namely we consider $G = \Gamma = 1$. The stabilization parameter is $\alpha = 0.1$ and the acceleration parameter is $\beta = -1$. Moreover, we set $\gamma = 2$ so that the target equilibrium is $F_\gamma = (2, 4)$.

In Figure 2 we show the phase portraits with the velocity field of the moment equations. The red lines are nullclines, and the gray-shaded area represents the unfeasible region where $E < m^2$. We observe that the stabilized version of the EKI proposed in this work preserves the target equilibrium F_γ . In the classical EKI, Figure 2a, the nullcline on the border of the feasible region is a set of equilibrium points. The stabilization moves these equilibria on the

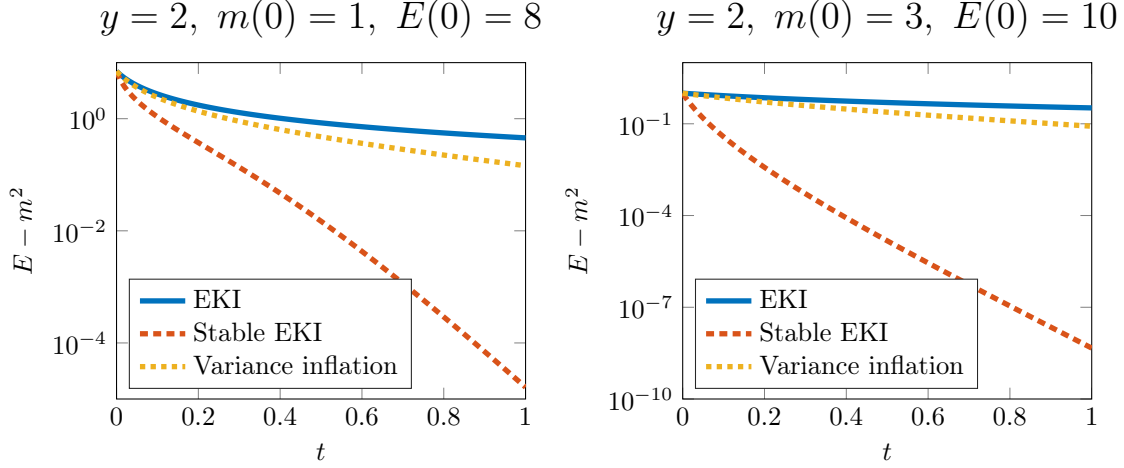


Figure 3: Variance evolution computed by solving the moment systems for the limit of the classical ensemble Kalman inversion (17), the stabilized ensemble Kalman inversion (24), and for the variance inflation (29) only, i.e. with $\beta = 0$. We consider two different sets of initial conditions.

red nullcline in the unfeasible region, see Figure 2b.

To provide additional numerical insight, we study the effect of the stabilization on the moment equations by looking at the time behavior of the covariance $C(t) = E - m^2$ for two different initial conditions in both systems, the limit of the classical EKI and the stabilized version. In addition, for a thorough comparison, we take into account also the dynamics presented in Section 3.3, obtained with a different variance inflation, cf. (29), and we consider $\beta = 0$, in order to highlight the effect of the acceleration term.

The initial conditions of the first moments are $m(0) = 1$ and $m(0) = 3$. The initial energy $E(0)$ is chosen such that $(m(0), E(0))$ is in the feasible region $C(0) \geq 0$. In Figure 3, we observe that all the methods show a variance decay to zero, i.e. collapse to a Dirac delta at mean-field level. However, noting the logarithmic scale in Figure 3 we see that the stable methods, characterized by variance inflation, decay to the equilibrium state much faster, precisely exponentially, than the limit of the classical EKI. Furthermore, we emphasize the role of the acceleration parameter β , which is taken into account only in the stable EKI method and which further speeds up the convergence speed.

4.2 A Two-Dimensional Inverse Problem

We consider the inverse problem of finding the hydraulic conductivity function of a non-linear elliptic equation in two spatial dimension assuming that noisy observation of the solution to the problem are available.

The problem is described by the following PDE modeling groundwater flow in a two-

dimensional confined aquifer:

$$(30) \quad \begin{aligned} -\nabla \cdot (e^{\log K} \nabla p) &= f \quad \text{in } \Omega = (-1, 1)^2 \\ p &= 0 \quad \text{on } \partial\Omega. \end{aligned}$$

Here, K is the hydraulic conductivity, f is the force function and the flow is described in terms of the piezometric head p . This problem has been intensively used in the literature on the ensemble Kalman inversion to study performance of the method. E.g. see [10, 23, 27].

We aim to find the log conductivity $u = \log K$ from 400 observations of the solution p on a uniform grid in Ω . We choose $f = 100$. The mapping from u to these observations is now non-linear, and thus we need to employ the ensemble dynamics for the non-linear model (21).

Noise is assumed to be Gaussian distributed with covariance $\Gamma^{-1} = \gamma^2 \mathbf{I}$, with $\gamma = 4$. The prior is also Gaussian distributed with covariance $(-\Delta)^{-2}$, whose discretization is again computed by using homogeneous Dirichlet boundary conditions. We use a \mathbb{P}^1 FEM approximation. The ensemble size is chosen as $J = 100$. The ensemble dynamics (21) are numerically solved by explicit Euler discretization with fixed and, to avoid stability issues, small time step $\Delta t = 10^{-3}$.

Final time for the simulations is determined by a stopping criterion in order to avoid over-fitting of the method, if not otherwise stated. We employ the discrepancy principle as stopping criterion. Thus, we check and stop the simulation when the condition $\vartheta \leq \|\eta\|^2$ is satisfied, where η is the measurement noise and

$$(31) \quad \vartheta = \frac{1}{J} \sum_{j=1}^J \|\mathcal{G}(\mathbf{u}^j) - \mathbf{p} - \eta\|^2$$

is the misfit which allows to measure the quality of the solution at each iteration. Moreover, \mathbf{u}^j and \mathbf{p} are vectors containing the discrete values of the control for the j -th ensemble member and of the true observations, respectively. In this example \mathcal{G} is the \mathbb{P}^1 FEM discretization of the continuous operator defining the elliptic PDE (30).

The initial ensemble is drawn from a Gaussian distribution with given covariance matrix $\delta(-\Delta)^{-2}$, and we consider $\delta = 1$ and $\delta = 10^{-2}$. We compare results obtained with the continuous-time limit of the classical EKI, i.e. when $\alpha = 1$ and $\beta = 0$, and with the stabilized method, using $\alpha = 0.9$ and $\beta = -1$.

In Figure 4 we show the time behavior of the misfit (31) (top row), of the residual (28) (middle row) and of the spread to the mean (27) (bottom row) provided by the two methods. The results in the left panels are obtained with $\delta = 1$, so that the initial ensemble is sampled from the same prior distribution of the exact control. The results in the center and right panels are computed with $\delta = 10^{-2}$, which mimics the situation of an overly confident prior, and hence with the covariance close to the border of the feasible region, at two different final times. More precisely, in the simulation depicted in the center column we allow the methods running until they meet the stopping criterion. Instead, in the right column we stop the simulations at time $T_{\text{fin}} = 1$, as the Bayesian interpretation of the method would suggest.

We observe that, if the distribution of the initial ensemble is properly chosen, i.e. when $\delta = 1$, the two methods meet the discrepancy principle, and the misfit, the residual and the ensemble spread monotonically decrease in time. However, while the limit of the classical

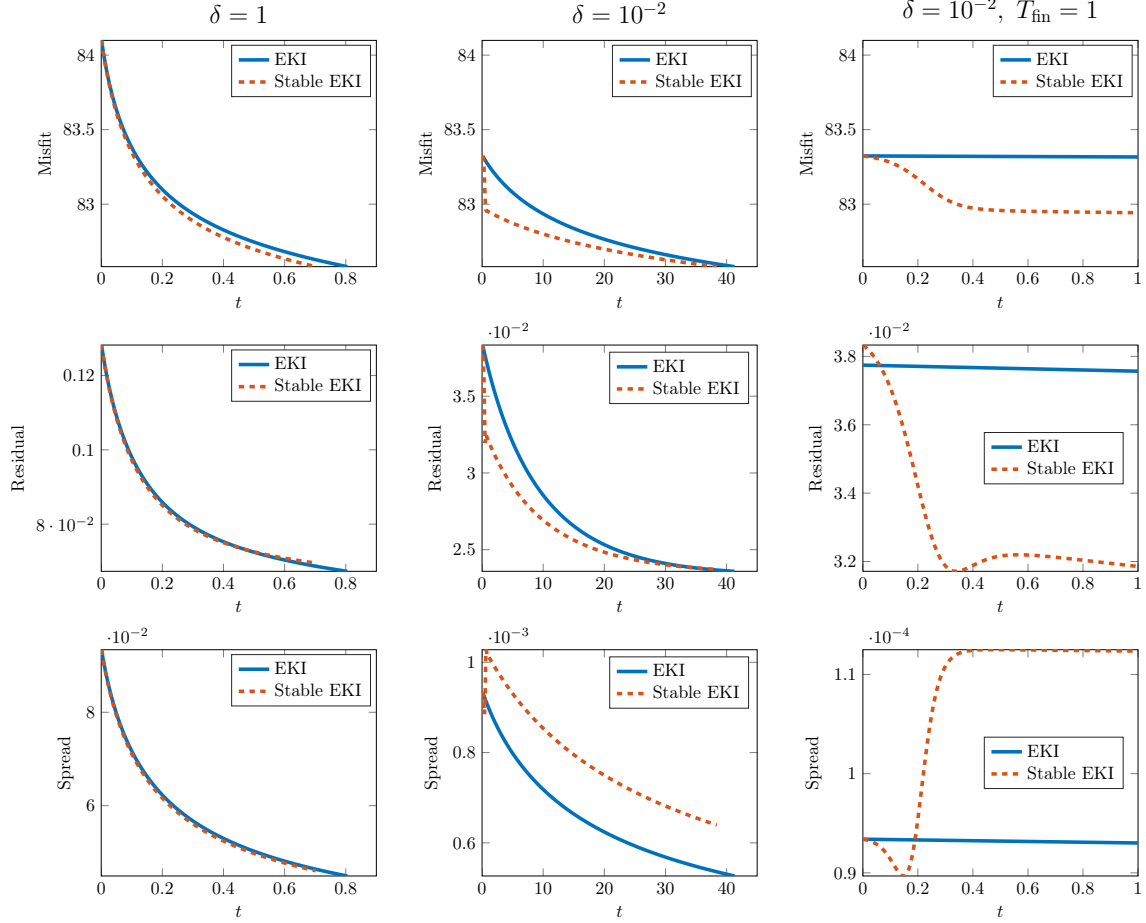


Figure 4: Misfit (31), residual (28) and spread (27) behavior in time for the inverse problem of determining the log conductivity $u = \log K$ for (30) using the classical ensemble Kalman inversion (EKI) (6) and the stabilized ensemble Kalman inversion (Stable EKI) (21). Left column: both methods converge for well chosen initial covariance ($\delta = 1$). Center and right columns represent the case of the overly confident prior, with $\delta = 10^{-2}$, up to the time when the discrepancy principle is met (center) and up to time $T_{\text{fin}} = 1$ (right).

EKI meets the stopping criterion at time $t \approx 0.8$, the stabilized version of the method stops at a time $t \approx 0.7$. Therefore, in this example the stabilization allows us to save about 12% of the computational cost. The difference between the two methods can be further appreciated when the initial guess of the ensemble is not properly chosen, i.e. when $\delta = 10^{-2}$. This is relevant in applications, where the distribution of the unknown control is not known, therefore the ensemble cannot be suitably initialized leading to a possible change in the length of the transient. We observe that the stabilized version of the method provides a fast transient of the misfit and of the residual when the final time is fixed to $T_{\text{fin}} = 1$. In contrast, the classical EKI which does not seem to converge. Hence, if we stop the simulation at $T_{\text{fin}} = 1$, as the Bayesian perspective suggests, the stabilized method provides a smaller misfit and residual. For long time behavior the limit of the classical EKI also converges, cf. the center column of Figure 4.

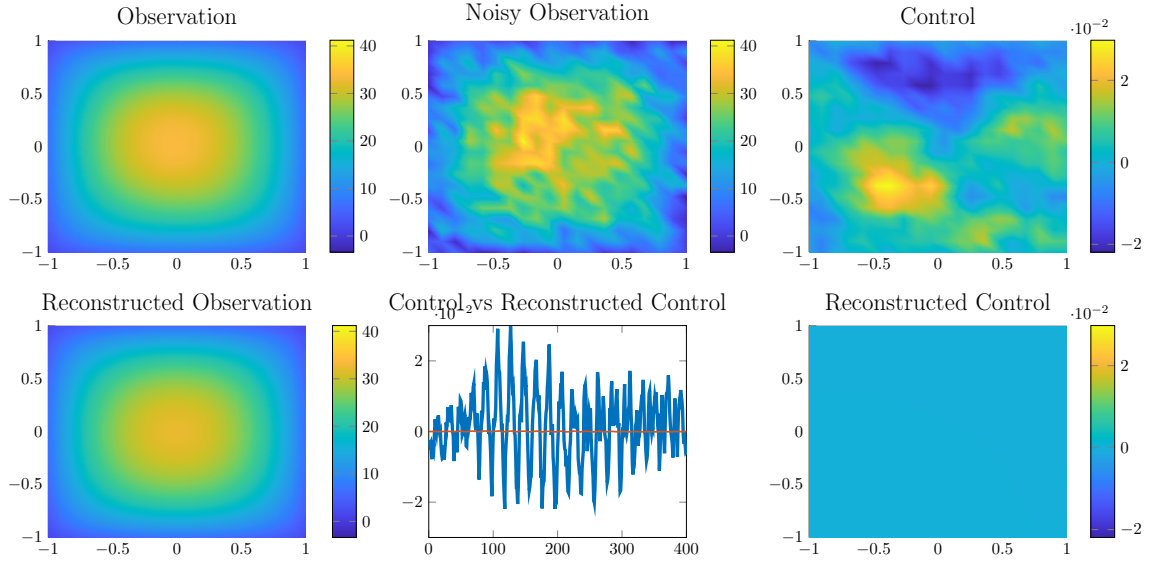


Figure 5: Inverse problem of determining the log conductivity $u = \log K$ for the two-dimensional groundwater equation (30) on a 20×20 grid, and solved by the continuous-time limit of the classical ensemble Kalman inversion (6). From top right: discrete observations of the true solution p ; true observations perturbed by Gaussian noise; discrete true log conductivity u ; solution computed with the identified unknown; one-dimensional plot of the discrete true and reconstructed log conductivity; discrete reconstructed log conductivity.

This is not surprising following the discussion in Section 2.4. The non-monotone behavior of the ensemble spread we observe in the right panel of the bottom row of Figure 4 can be explained by the fact that the initial ensemble is already close to collapse.

The effect on the performance of the methods when considering an overly initial ensemble can be also observed by comparing the results in Figure 5, referred to the classical ensemble Kalman inversion, and in Figure 6, for the stabilized version of the method. Thus, we consider the case $\delta = 10^{-2}$ only. In both situations, we stop the simulation at time $T_{\text{fin}} = 1$. The top-row panels of both figures are the same. They show, from left to right, the true solution p of (30) evaluated on a 20×20 uniform grid, the perturbed solution by additive Gaussian noise, and the a-priori artificially assigned true log conductivity u , i.e. the control in this example, which provides the solution p and we aim to identify. The bottom-row panels, instead, show the solution obtained with the reconstructed log conductivity, and the identified control itself using both a one-dimensional and a two-dimensional visualization. In these figures we appreciate the importance of the distribution of the initial ensemble in order to ensure that the classical method, i.e. when covariance inflation and regularization terms are not considered, is able to provide a good identification of the unknown control.

5 Discussion and conclusions

The important point of this manuscript is the observation that the EKI leads to structurally unstable dynamical moment systems. This has technical aspects, like the fact that the target

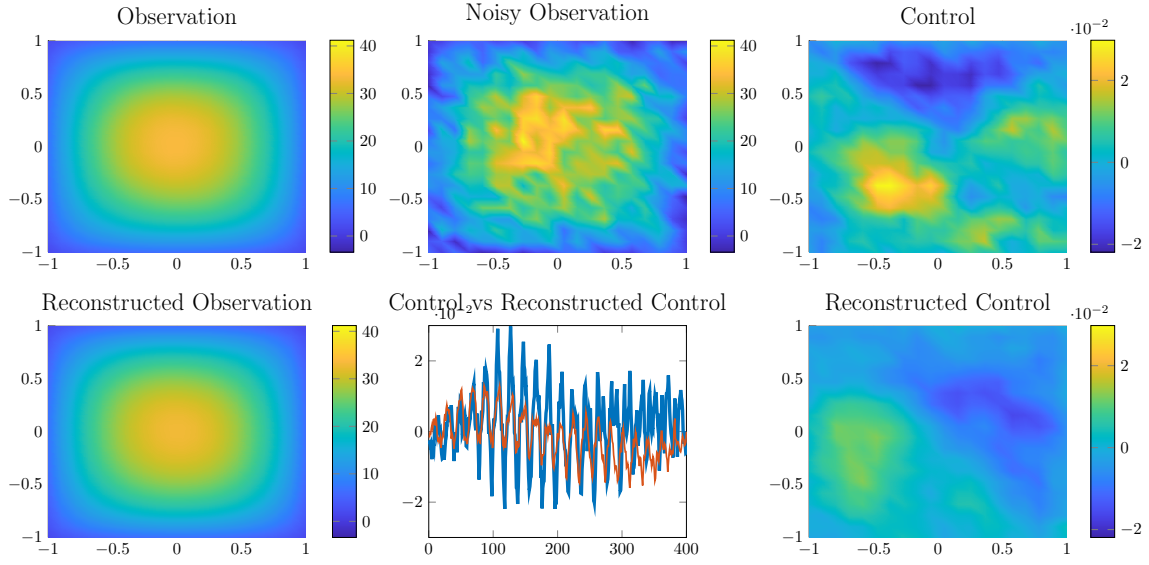


Figure 6: Inverse problem of determining the log conductivity $u = \log K$ for the two-dimensional groundwater equation (30) on a 20×20 grid, and solved by the stabilized ensemble Kalman inversion method (21) with $\alpha = 0.9$ and $\beta = -1$. From top right: discrete observations of the true solution p ; true observations perturbed by Gaussian noise; discrete true log conductivity u ; solution computed with the identified unknown; one-dimensional plot of the discrete true and reconstructed log conductivity; discrete reconstructed log conductivity

equilibrium is unstable from the unfeasible side of the phase space and that it is, while stable, approached only very slowly in time. However, this is also conceptually very important: Typically mathematical models that lead to structurally unstable dynamical systems are flawed – the modeling part missed important aspects making the analysis of the resulting dynamical system highly susceptible to small noise and small variations in the model. A classical example is provided by chemical reactor modeling, see [30].

Conventional wisdom is that the modeling leading to the structurally unstable system should be re-examined and it should be determined whether there are legitimate reasons (like in the case of Hamiltonian systems or systems with inherent symmetries) for the structural instability or whether the modeling process lead to the structurally unstable result.

Due to the appeal of the EKI it is important to understand where the conceptual issue of a structurally unstable dynamical systems comes from. We have done that in this paper and shown that by computing the continuum limit of the classical EKI, terms are lost that lead to the structural instability. We also show how to make the EKI structurally stable. The stabilization relies on a suitable inflation of the covariance operator which makes the target equilibrium globally asymptotically stable, and thus approached exponentially fast in time. The numerical results illustrate that the stabilized method is able to provide fast convergence to the solution, independently of the choice of the distribution for the initial ensemble.

References

- [1] S. I. Aanonsen, G. Naevdal, D. S. Oliver, A. C. Reynolds, and B. Valles. The ensemble Kalman filter in reservoir engineering—a review. *SPE J.*, 14(3):393–412, 2009.
- [2] D. J. Albers, P.-A. Blancquart, M. E. Levine, E. E. Seylabi, and A. M. Stuart. Ensemble Kalman methods with constraints. *Inverse Probl.*, 35(9):095007, 2019.
- [3] J. L. Anderson. An Ensemble Adjustment Kalman Filter for Data Assimilation. *Monthly Weather Review*, 129(12):2884–2903, 2001.
- [4] K. Bergemann and S. Reich. An ensemble Kalman-Bucy filter for continuous data assimilation. *Meteorologische Zeitschrift*, 21(3):213–219, 2012.
- [5] D. Bloemker, C. Schillings, and P. Wacker. A strongly convergent numerical scheme from ensemble Kalman inversion. *SIAM J. Numer. Anal.*, 56(4):2537–2562, 2018.
- [6] D. Bloemker, C. Schillings, P. Wacker, and S. Weissman. Well Posedness and Convergence Analysis of the Ensemble Kalman Inversion. *Inverse Probl.*, 35(8), 2019.
- [7] J. A. Carrillo, M. Fornasier, G. Toscani, and F. Vecil. *Mathematical Modeling of Collective Behavior in Socio-Economic and Life Sciences*, chapter Particle, kinetic, and hydrodynamic models of swarming, pages 297–336. Modeling and Simulation in Science, Engineering and Technology. Birkhäuser Boston, 2010.
- [8] J. A. Carrillo and U. Vaes. Wasserstein stability estimates for covariance-preconditioned Fokker-Planck equations. *Nonlinearity*, 34(4):2275, 2021.
- [9] N. K. Chada. Limit analysis of hierarchical ensemble Kalman inversion. *J. Inverse Ill-Posed Probl.*, 2020. In press.
- [10] N. K. Chada, A. M. Stuart, and X. T. Tong. Tikhonov regularization within ensemble Kalman inversion. *SIAM J. Numer. Anal.*, 58(2):1263–1294, 2020.
- [11] Y. Chen and D. S. Oliver. Parameterization techniques to improve mass conservation and data assimilation for ensemble Kalman filter. SPE Western Regional Meeting, 2010.
- [12] Z. Ding and Q. Li. Ensemble Kalman Inversion: mean-field limit and convergence analysis. *Stat. Comput.*, 31:9, 2021.
- [13] Z. Ding, Q. Li, and J. Lu. Ensemble Kalman inversion for nonlinear problems: Weights, consistency, and variance bounds. *Found. Data Sci.*, 3(3):371–411, 2021.
- [14] A. A. Emerick and A. C. Reynolds. Ensemble smoother with multiple data assimilation. *Computers and Geosciences*, 55:3–15, 2013.
- [15] G. Evensen. Sequential data assimilation with a nonlinear quasi-geostrophic model using Monte Carlo methods to forecast error statistics. *J. Geophys. Res.*, 99:10143–10162, 1994.

- [16] G. Evensen and P. J. Van Leeuwen. Assimilation of geosat altimeter data for the agulhas current using the ensemble Kalman filter with a quasi-geostrophic model. *Monthly Weather*, 128:85–96, 1996.
- [17] A. Garbuno-Inigo, F. Hoffmann, W. Li, and A. M. Stuart. Interacting Langevin Diffusions: Gradient Structure and Ensemble Kalman Sampler. *SIAM J. Appl. Dyn. Syst.*, 19(1):412–441, 2020.
- [18] John Guckenheimer and Philip Holmes. *Nonlinear oscillations, dynamical systems, and bifurcations of vector fields*, volume 42. Springer Science & Business Media, 2013.
- [19] S.-Y. Ha and E. Tadmor. From particle to kinetic and hydrodynamic descriptions of flocking. *Kinet. Relat. Models*, 3(1):415–435, 2008.
- [20] E. Haber, F. Lucka, and L. Ruthotto. Never look back - A modified EnKF method and its application to the training of neural networks without back propagation. Preprint arXiv:1805.08034, 2018.
- [21] M. Herty and G. Visconti. Kinetic methods for inverse problems. *Kinet. Relat. Models*, 12(5):1109–1130, 2019.
- [22] M. Herty and G. Visconti. Continuous limits for constrained ensemble Kalman filter. *Inverse Probl.*, 2020.
- [23] M. Iglesias, K. Law, and A. M. Stuart. Ensemble Kalman methods for inverse problems. *Inverse Probl.*, 29(4):045001, 2013.
- [24] T. Janjić, D. McLaughlin, S. E. Cohn, and M. Verlaan. Conservation of mass and preservation of positivity with ensemble-type Kalman filter algorithms. *Monthly Weather Review*, 142(2):755–773, 2014.
- [25] N. B. Kovachki and A. M. Stuart. Ensemble Kalman inversion: a derivative-free technique for machine learning tasks. *Inverse Probl.*, 35(9):095005, 2019.
- [26] L. Pareschi and G. Toscani. *Interacting Multiagent Systems. Kinetic equations and Monte Carlo methods*. Oxford University Press, 2013.
- [27] C. Schillings and A. M. Stuart. Analysis of the Ensemble Kalman Filter for Inverse Problems. *SIAM J. Numer. Anal.*, 55(3):1264–1290, 2017.
- [28] C. Schillings and A. M. Stuart. Convergence analysis of ensemble Kalman inversion: the linear, noisy case. *Appl. Anal.*, 97(1):107–123, 2018.
- [29] M. Schwenzer, G. Visconti, M. Ay, T. Bergs, M. Herty, and D. Abel. Identifying trending coefficients with an ensemble Kalman filter. *IFAC-PapersOnLine*, 53(2):2292–2298, 2020.
- [30] S. Serra and C. Tablino Possio. Analytical analysis of the Gavrilov-Guckenheimer bifurcation unfolding in the case of a proportional-integral controlled CSTR. *SIAM J. Appl. Math.*, 59(5):1716–1744, 1999.
- [31] B. O. S. Teixeira, L. A. B. Târres, L. A. Aguirre, and D. S. Bernstein. On unscented Kalman filtering with state interval constraints. *J. Process Contr.*, 20(1):45–57, 2010.

- [32] X. T. Tong, A. J. Majda, and D. Kelly. Nonlinear stability of the ensemble Kalman filter with adaptive covariance inflation. *Commun. Math. Sci.*, 14(5):1283–1313, 2016.
- [33] G. Toscani. Kinetic models of opinion formation. *Commun. Math. Sci.*, 4(3):481–496, 2006.
- [34] X.-L. Zhang, C. Michelén-Ströfer, and H. Xiao. Regularized ensemble Kalman methods for inverse problems. *J. Comput. Phys.*, 416:109517, 2020.